analytical chemistry

pubs.acs.org/ac

Article

Diffusion and Relaxation Edited Proton NMR Spectroscopy of Plasma Reveals a High-Fidelity Supramolecular Biomarker Signature of SARS-CoV-2 Infection

Samantha Lodge, Philipp Nitschke, Torben Kimhofer, Julien Wist, Sze-How Bong, Ruey Leng Loo, Reika Masuda, Sofina Begum, Toby Richards, John C. Lindon, Wolfgang Bermel, Tony Reinsperger, Hartmut Schaefer, Manfred Spraul, Elaine Holmes,* and Jeremy K. Nicholson*

Cite This: *Anal. Chem.* 2021, 93, 3976–3986

Read Online

ACCESS | Metrics & More | Article Recommendations | Supporting Information

ABSTRACT: We have applied nuclear magnetic resonance spectroscopy based plasma phenotyping to reveal diagnostic molecular signatures of SARS-CoV-2 infection *via* combined diffusional and relaxation editing (DIRE). We compared plasma from healthy age-matched controls (n = 26) with SARS-CoV-2 negative non-hospitalized respiratory patients and hospitalized respiratory patients (n = 23 and 11 respectively) with SARS-CoV-2 rRT-PCR positive respiratory patients (n = 17, with longitudinal sampling time-points). DIRE data were modelled using principal component analysis and orthogonal projections to latent structures discriminant analysis (O-PLS-DA), with statistical cross-validation indices indicating excellent model generalization for the classification of SARS-CoV-2 positivity for all comparator groups (area under the receiver operator characteristic curve = 1). DIRE spectra show biomarker signal combinations conferred by differential concentrations of metabolites with selected molecular mobility properties. These comprise the following: (a) composite *N*-acetyl signals from α-1-acid glycoprotein and other glycoproteins (designated GlycA and GlycB) that were elevated in SARS-CoV-2 positive patients [$p = 2.52 \times 10^{-10}$ (GlycA) and 1.25×10^{-9} (GlycB) *vs* controls], (b) two diagnostic supramolecular phospholipid composite signals that were identified (SPC-A and SPC-B) from the $-^{+}N-(CH_3)_3$ choline headgroups of lysophosphatidylcholines carried on plasma glycoproteins and from phospholipids in high-density lipoprotein subfractions (SPC-A) together with a phospholipid component of low-density lipoprotein (SPC−B). The integrals of the summed SPC signals (SPC_{total}) were reduced in SARS-CoV-2 positive patients relative to both controls ($p = 1.40 \times 10^{-7}$) and SARS-CoV-2 negative patients ($p = 4.52 \times 10^{-8}$) but were not significantly different between controls and SARS-CoV-2 negative patients. The identity of the SPC signal components was determined using one and two dimensional diffusional, relaxation, and statistical spectroscopic experiments. The SPC_{total}/GlycA ratios were also significantly different for control *versus* SARS-CoV-2 positive patients ($p = 1.23 \times 10^{-10}$) and for SARS-CoV-2 negatives *versus* positives ($p = 1.60 \times 10^{-9}$). Thus, plasma SPC_{total} and SPC_{total}/GlycA are proposed as sensitive molecular markers for SARS-CoV-2 positivity that could effectively augment current COVID-19 diagnostics and may have value in functional assessment of the disease recovery process in patients with long-term symptoms.

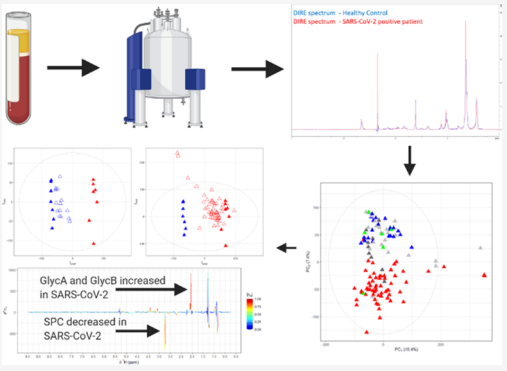

INTRODUCTION

The COVID-19 disease pandemic resulting from SARS-CoV-2 infection has so far resulted in over 101 million cases and 2.4 million deaths worldwide. The range of clinical expression of COVID-19 is extreme, varying from asymptomatic or mild to severe respiratory distress and multiple organ damage, with or without respiratory involvement. There is an unmet need for accurate diagnosis and prediction of disease severity at an early stage so that individual infections can be monitored and managed effectively. There is also a need for new functional markers of patient recovery in COVID-19, especially for classifying the complex systemic complications of the disease. Hence, we applied biofluid metabolic phenotyping to COVID-19 as these approaches have previously given deep insights into a range of pathological processes that can be modelled using multivariate statistical methods to achieve classification of disease subtypes and detection of novel biomarkers.[1,2]

We recently proposed an extension to the *metabolic phenoconversion* concept to explore the systemic shifts in plasma

Received: November 25, 2020
Accepted: January 28, 2021
Published: February 12, 2021

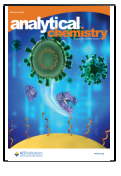

biochemistry resulting from SARS-CoV-2 infection and the accompanying multisystem pathological disruptions caused by the virus.[3] Phenoconversion for COVID-19 is associated with changes to a range of metabolic biomarkers (lipoproteins glycoproteins, amino acids, lipids, and other metabolites) that can be derived from nuclear magnetic resonance (NMR) spectroscopic and mass spectrometric data. Indeed, combining NMR and mass spectrometry-generated metabolic features into an integrated supervised classification model allowed excellent discrimination between SARS-CoV-2 positive from control participants.[3] This approach also enabled deep insights to be gained into the systemic nature of the COVID-19 disease, with its distinctive embedded biomarker features including those previously observed in diabetes, cardiovascular disease, liver dysfunction, neurological disruption, and acute inflammation.[3] Proton NMR spectroscopy has been shown to be highly effective in detecting disease signatures in biofluids such as blood plasma,[4−7] and multiple NMR methods have been applied to extract latent biomarker information either using physical NMR experiments including two-dimensional (2D) methods[8] or Statistical Total Correlation Spectroscopy total correlation spectroscopy (STOCSY) and related techniques.[9−11] Although physical procedures can be used to extract, separate, and augment detection and identification of metabolites[12] and lipoproteins in plasma,[13] one of the key advantages of NMR spectroscopy is its non-invasive and non-destructive nature, which enables the interrogation of molecular interaction complexation and physical dynamics of complex mixtures that can carry extra diagnostic information.[5]

Plasma glycoproteins are biosynthesized and released mainly from the liver; they are enzymatically glycosylated and assist solubilization of multiple hydrophobic compounds in the blood.[14] We and others have reported that the well-resolved *N*-acetyl signals from glycosylated amino sugar residues in acute phase-reactive proteins such as α-1-*N*-acetyl-glycoprotein in the NMR spectra of blood plasma are elevated in multiple inflammatory states, including obesity,[15] diabetes,[16] cardiovascular disease,[17] rheumatoid arthritis,[18] and systemic immune-pathological conditions such as HIV infection[19,21] and systemic lupus erythematosus[20] (Supporting Information Table S1).[19] These signals have had various designations over the years but are now widely described as GlycA and GlycB.[21,22] The GlycA signal (δ 2.03) is a composite of *N*-acetyl signals from five proteins: α-1-acid glycoprotein (the strongest component), α-1-antichymotrypsin, α-1-antitrypsin, haptoglobin, and transferrin.[21] In α-1-acid glycoprotein, the signal originates from five *N*-linked oligosaccharide chains on a backbone of 183 amino acid residues and is present at approximately 20 μM in healthy individuals.[22] The α-1-acid glycoprotein has the strongest correlation with the GlycA signal and is thought to account for most of the signal, although inter-individual differences in the levels of these five glycoproteins have been reported.[19] Multiple biological functions have been ascribed to α-1-acid glycoprotein including modulating immunological function *via* a macrophage-released inhibitory factor that acts to prevent IL-1 activation of thymocyte proliferation,[23] stimulation of lymphocyte proliferation,[24] serving as drug transporters, and inhibition of platelet aggregation.[25−27] Acute phase inflammation has been associated with 2 to 5-fold increases in plasma GlycA signals.[28] The GlycB acetyl signal (δ 2.07) arising from glycoprotein *N*-acetylneuraminidino groups has also been observed to increase in various inflammatory conditions such as diabetes and obesity.[29] Both GlycA and GlycB have been shown to correlate with C-reactive protein (CRP) levels in plasma,[17] and it has been suggested that GlycA and GlycB may be superior biomarkers of systemic inflammation over CRP, the main clinical chemistry marker of inflammation.[19,29] We recently reported that GlycA and GlycB are significantly elevated in COVID-19 patients and are strong markers of disease positivity.[3]

The nondestructive nature of NMR allows the study of complex supramolecular structures in the natural state in multiphasic samples such as blood plasma.[5] The proton T_2 relaxation properties allow for differential spectral editing for instance to remove broad macromolecular envelopes in blood or plasma based on their short proton T_2's.[30] Translational diffusion can also be measured using pulsed field gradients and this technique can be used to remove NMR peaks from small molecules that have rapid translational motion. The original NMR experiment for measuring diffusion constants is the "stimulated echo experiment"; and this is now most commonly applied as the pseudo-two-dimensional method known as DOSY.[31−33] It is also possible to combine motional editing in 2D experiments such as diffusion-edited total correlation spectroscopy (DE-TOCSY[34] or both types of motional editing together including DIffusion and Relaxation Editing (DIRE).[35] We have previously shown that DIRE spectra enhance signals from molecules with slow translational diffusion but with high segmental motional freedom, and these requirements are satisfied by plasma glycoproteins and molecules constrained within certain lipoprotein subcompartments. So, in order to study the role of GlycA and GlycB as composite markers of SARS-CoV-2 infection further, we applied DIRE NMR experiments to SARS-CoV-2-positive and negative patients as well as samples from controls and observed a unique diagnostic pattern, involving Glyc and bound phospholipids, that distinguishes SARS-CoV-2 positive samples from others with high fidelity.

MATERIALS AND METHODS

Patient Enrolment and Sample Collection. Blood plasma samples were collected into lithium heparin sample tubes from a cohort of adult individuals in a study initiated at the Fiona Stanley Hospital in the Western Australia South Metropolitan Health Service catchment as part of the International Severe Acute Respiratory and Emerging Infection Consortium/World Health Organization pandemic trail framework (SMHS Research Governance Office PRN: 3976 and Murdoch University Ethics no. 2020/052). Healthy control participants were enrolled as volunteers and provided study details. A written informed consent was obtained prior to data collection in accordance with the ethical governance (Murdoch University Ethics no. 2020/053). Five groups of participants were recruited from the Fiona Stanley and Royal Perth Hospitals: (i) patients who presented with COVID-19 disease symptoms and subsequently tested positive for SARS-CoV-2 infection from upper and/or lower respiratory tract swabs by RT-polymerase chain reaction (PCR) (n = 17 patients, sampled at various times resulting in n = 58 plasma specimens); (ii) healthy controls who had not exhibited COVID-19 disease symptoms (n = 26 participants); (iii) individuals with respiratory disease symptoms and who tested negative for SARS-CoV-2 and were non-hospitalized (n = 23 participants); (iv) hospitalized SARS-CoV-2 negative respiratory patients (n = 11); (v) individuals who were serologically IgA positive for COVID-19 (n = 6). Serological testing for SARS-CoV-2 antibodies was performed at the PathWest clinical testing

https://dx.doi.org/10.1021/acs.analchem.0c04952
Anal. Chem. 2021, 93, 3976−3986

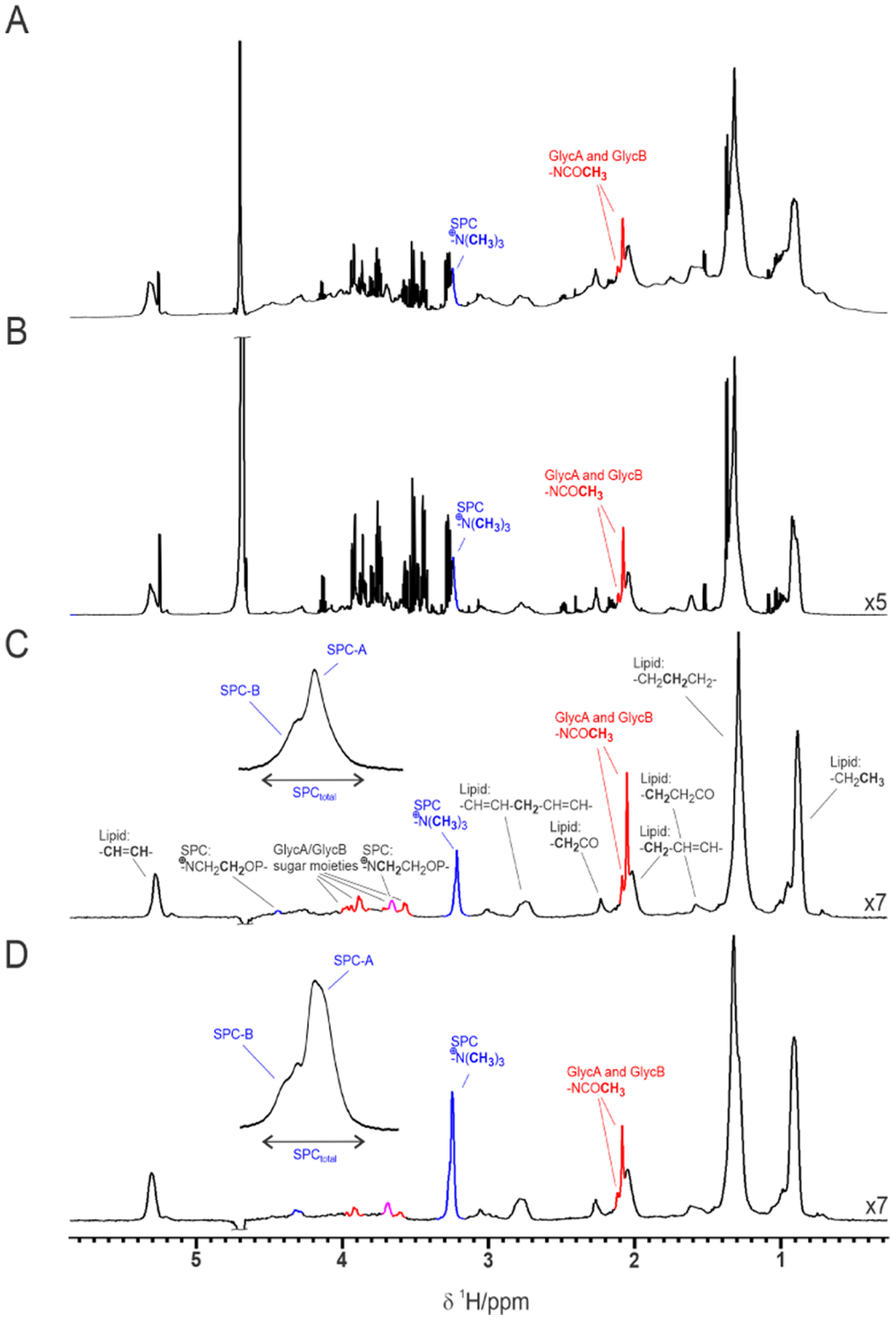

Figure 1. Stacked 600 MHz ^{1}H NMR plot showing (A) standard water-suppressed 1D NMR spectrum of plasma from a typical SARS-CoV-2 positive patient, (B) water-suppressed CPMG spin-echo spectrum; (C) DIRE spectrum of the same sample, and (D) DIRE spectrum of the plasma from a representative healthy control individual. The lipid peaks are labelled according to chemical structure rather than from their lipoprotein components. In DIRE spectra (c,d), these composite lipidic signals are dominantly from phosphatidylcholine and other phospholipids in HDL bound to glycoprotein and to a lesser extent LDL. The main DIRE COVID-19 discriminating peaks are highlighted in red (representing *N*-acetylglycoprotein signals GlycA and GlycB); blue SPC (which refers to a supramolecular phospholipid composite $-N^+(CH_3)_3$ signal); magenta (overlapping contribution from both *N*-acetylglycoproteins and SPC). SPC_{total} refers to the integrated signal from the choline head groups in the SPC shown in the ratio calculations and used in Table 1.

laboratories, Western Australia using 10 μL of plasma in a commercial point-of-care serological COVID-19 IgA/IgG test. Samples were considered as SARS-CoV-2 positive if IgA >1.0 or equivocal where IgA = 0.8−1.0. Demographic data together with the clinical symptoms are shown in Supporting Information Tables S2−S4. IgA and IgG levels are reported in Table S5. Plasma samples were stored at −80 °C until required for analysis.

https://dx.doi.org/10.1021/acs.analchem.0c04952
Anal. Chem. 2021, 93, 3976−3986

Sample Processing. Plasma samples were thawed at 20 °C for 30 min and then centrifuged at 13,000*g* for 10 min at 4 °C. Plasma samples were prepared in 5 mm outer diameter SampleJet NMR tubes following the recommended procedures for *in vitro* analytical and diagnostics procedures[37] using 300 μL of plasma mixed with 300 μL of phosphate buffer (75 mM Na_2HPO_4, 2 mM NaN_3, and 4.6 mM sodium trimethylsilyl propionate-[2,2,3,3-2H_4] (TSP) in 80% D_2O, pH 7.4 ± 0.1). NMR SampleJet tubes were sealed with POM balls added to the caps. All processing procedures were compliant with our previous recommendations on sample handling and storage for COVID-19 samples.[38]

600 MHz Proton NMR Spectroscopy and *In Vitro* Diagnostic Experiments. NMR spectroscopic analyses were performed on a 600 MHz Bruker Avance III HD spectrometer equipped with a 5 mm BBI probe and fitted with the Bruker SampleJet robot cooling system set to 5 °C. A full quantitative calibration was completed prior to the analysis using a previously described protocol.[36] A series of NMR experiments were performed, comprising the Bruker's *in vitro* diagnostics research (IVDr) method set: (i) a standard 1D experiment with solvent presaturation, (ii) a Carr−Purcell−Meiboom−Gill (CPMG) spin-echo experiment, and (iii) a 2D J-resolved experiment. The total experiment time was 12.5 min per sample. Data were processed in the automation mode using Bruker Topspin 3.6.2 and ICON NMR to achieve phasing, baseline correction, and calibration to TSP. Further regression experiments were performed to quantify 112 parameters of main plasma lipoprotein classes and subclasses (Bruker IVDr lipoprotein subclass analysis, B.I.-LISA) based on a PLS-regression model using the $-(CH_2)_n$ (δ 1.25) and $-CH_3$ (δ 0.80) signals.[37]

DIRE NMR Experiments. Given that GlycA and GlycB signals were markedly increased in COVID-19 positive patients[3] and that we previously observed glycoprotein signals in the DIRE spectra of normal human plasma,[35] we decided to apply this approach to further investigate its diagnostic potential for assessment of SARS-CoV-2 positivity. A series of four new DIRE pulse sequences were designed and tested each with various irradiation and gradient modifications from the original DIRE experiment (here designated as DIRE-1, see the Supporting Information), all giving broadly similar levels of spectroscopic classification and performance for detecting SARS CoV-2 positivity; these are described in the Supporting Information (Figure S3). In full automation, the acquisition time amounted to 4.5 min per sample. The DIRE variant employed in the current studies replaced the modified WATERGATE[35] solvent suppression sequence used in the original DIRE experiment with a continuous secondary irradiation field at the water resonance frequency. For simplicity, we refer to this new sequence simply as DIRE throughout the subsequent text. To aid signal assignment, we performed 2D NMR methods and model phospholipid titrations into plasma, as described in the Supporting Information.

Data Preprocessing and Statistical Evaluation. One-dimensional (1D) spectral data preprocessing comprised the excision of the residual water resonances (δ 4.5−5.0) and chemical shift regions where no signals were observed (δ < 0.25 and δ > 9.5). The chemical shift axis was calibrated to the α-anomeric proton of glucose (δ 5.23). The chemical shift calibration of the DIRE spectra was achieved using the α anomeric proton signal from glucose in the sample matched CPMG spectrum, whereas DIRE and CPMG spectra were acquired under identical analytical conditions for each sample. We tested other different DIRE calibration options using DIRE signals as calibrants; however, spectral calibration with the glucose signal of the CPMG spectra from the same sample proved optimal. Spectra were baseline-corrected using an asymmetric least-squares method. To aid the assignment of structural information relating to DIRE signals δ 2.03 (GlycA) and δ 3.20−3.30 [Supramolecular Phospholipid Composite (SPC)], we applied 1D STOCSY using the DIRE spectra from all study groups (healthy controls and patients with and without SARS-CoV-2 infection). Statistical evaluation was performed with principal components analysis (PCA) as an unsupervised multivariate method, compressing the high-dimensional spectral data set into a few latent variables, thereby establishing potential sample clustering trends based on the covariance structure. Group comparison was performed using orthogonal projections to latent structures-discriminant analysis (O-PLS-DA) using a training set of seven SARS-CoV-2 positive and seven age and sex matched healthy controls. The optimal number of components (one predictive + one orthogonal) in the model was established using the area under the receiver operator characteristic curve (AUROC) as the model generalization index, computed in a jack-knifing statistical cross-validation framework. Data were mean-centered and scaled to unit variance prior to multivariate modelling. All data analysis tasks were performed in the statistical programming language R, using the *metabom8* package (V 0.2), obtainable at https://github.com/tkimhofer. In order to evaluate associations between GlycA, GlycB, SPC, and plasma lipoproteins measured by IVDr,[3] a Spearman's correlation analysis was performed using respective signal integrals. Results were visualized as heatmaps;[38] rows and columns were ordered according to lipoprotein density classes.

RESULTS AND DISCUSSION

NMR Spectra of Blood Plasma. Typical water-suppressed 1D, spin-echo, and DIRE spectra of plasma (control plus patient) are shown in Figure 1. The DIRE ^{1}H NMR spectra provide an observational window on molecules and structures with slow translational diffusion but high levels of segmental motion (long T_2 relaxation times), capturing the compositional differences in certain plasma glycoprotein and lipoprotein subcompartments (Figure 1C,D). Thus, in comparison to the standard 1D 600 MHz ^{1}H NMR water-suppressed spectra (Figure 1A), which are dominated by broad envelopes of macromolecular resonances with superimposed sharp signals mainly from low-molecular-weight metabolites, it is easier to see the contributions from *N*-acetyl glycoproteins and selected compartmentalized lipoprotein signals. With respect to molecular information, the DIRE spectra, in which signals from molecules with rapid translational diffusion are eliminated, are almost the reverse to the CPMG spin-echo spectra (Figure 1B) that only carry information on sharp line signals from protons with long T_2 relaxation times.[8,30] While standard 1D and CPMG pulse sequences have previously been applied to blood plasma in multiple physiological and pathological studies to extract molecular biomarker information,[5,8,30,34,39] diffusion-edited spectroscopy has been less frequently applied in a diagnostic setting.[33,40] DIRE spectroscopy to our knowledge has only been demonstrated in principle as a spectral editing tool, but not so far applied to study disease diagnostics or systemic pathology. Here, the normal healthy and SARS-CoV-2 positive samples were significantly different based on their DIRE NMR signatures, with increased intensity of the GlycA and GlycB

https://dx.doi.org/10.1021/acs.analchem.0c04952
Anal. Chem. 2021, 93, 3976−3986

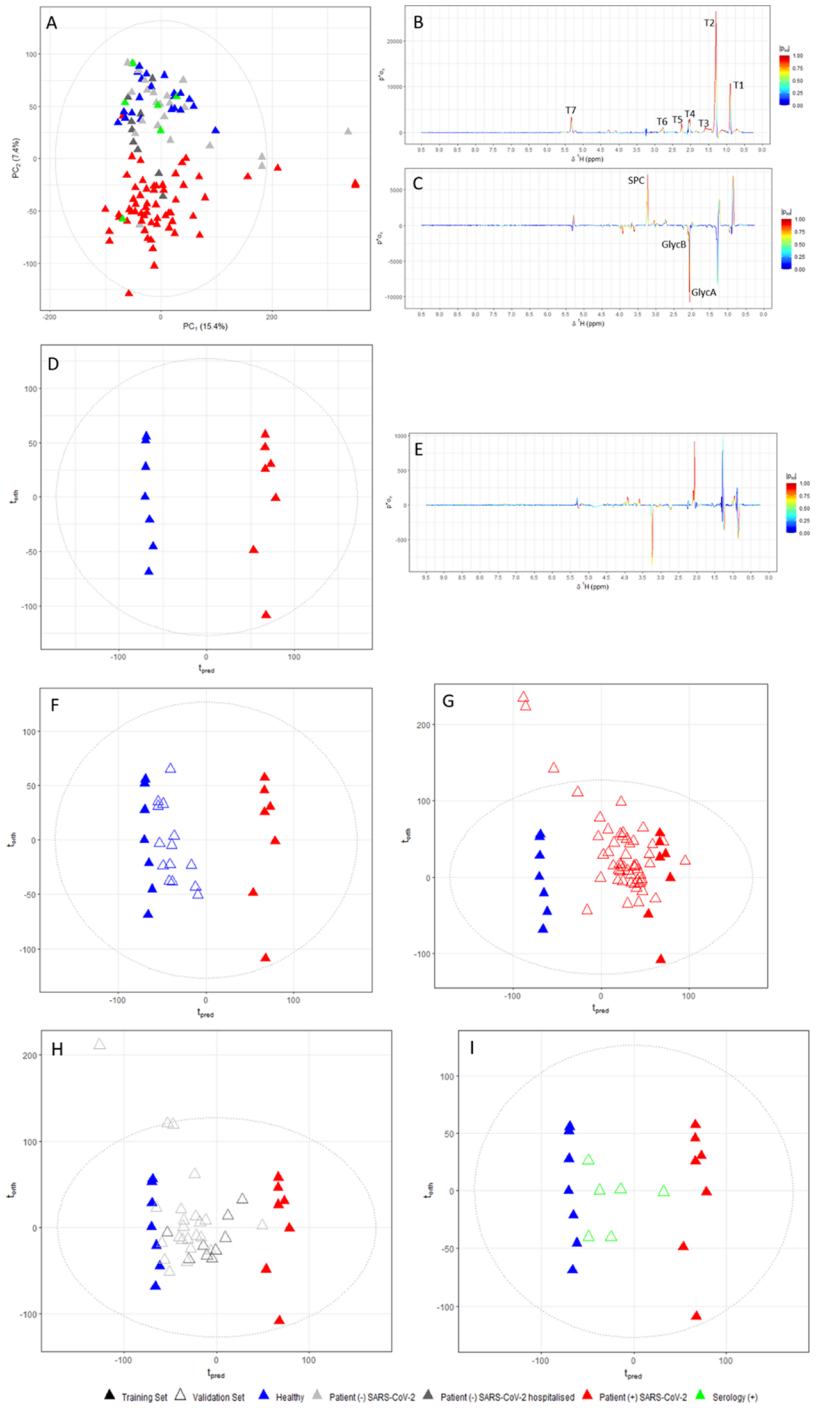

Figure 2. (A) PCA of the DIRE spectra of healthy controls (blue triangles), SARS-CoV-2-positive patients (red triangles), SARS-CoV-2-negative nonhospitalized patients (light gray triangles), SARS-CoV-2-negative hospitalized patients (dark gray triangles), and serology (+) participants (green triangles). The ellipse in panel A indicates the Hotelling's T2 statistic ($\alpha = 0.95$), which can be interpreted as the multivariate confidence interval. (B) Loadings of PC 1 of panel (A). Triglyceride signals are labelled (T1−T7). T1: $-CH_2\mathbf{CH_3}$ T2: $-CH_2-\mathbf{CH_2}-CH_2-$ T3: $-\mathbf{CH_2}-CH_2-CO$ T4: $-\mathbf{CH_2}-CH{=}CH-$ T5: $-\mathbf{CH_2}CO$ T6: $-CH{=}CH-\mathbf{CH_2}-CH{=}CH-$ T7: $-\mathbf{CH{=}CH}-$. Loadings of PC 2 of panel (A). (D) DIRE OPLS-DA plot showing the training model consisting of SARS-CoV-2-positive patients ($n = 7$), age and sex matched to the healthy control group ($n = 7$). (E) OPLS-DA loadings of the training model. (F) OPLS-DA plot showing the training model with the healthy control samples ($n = 19$) projected into the model. (G) DIRE OPLS-DA plot showing the training model with the SARS-CoV-2-positive patients ($n = 51$ samples) projected into the model. (H) DIRE OPLS-DA plot showing the training model with the SARS-CoV-2-negative patients ($n = 34$) projected into the model. (I) DIRE OPLS-DA plot showing the training model with the projected serology (+) participants ($n = 6$).

signals and decreased intensity of a cluster of choline head group signals at δ 3.20−3.30.

Multivariate Statistical Analysis of DIRE NMR Spectra. PCA of the DIRE spectra for SARS-CoV-2 PCR positives, healthy, and SARS-CoV-2 PCR negatives together with spectra from seropositive individuals who did not undergo PCR testing for SARS-CoV-2 infection show a nonoverlapping distribution for SARS-CoV-2 positives (red) *versus* healthy (blue), with

https://dx.doi.org/10.1021/acs.analchem.0c04952
Anal. Chem. 2021, 93, 3976−3986

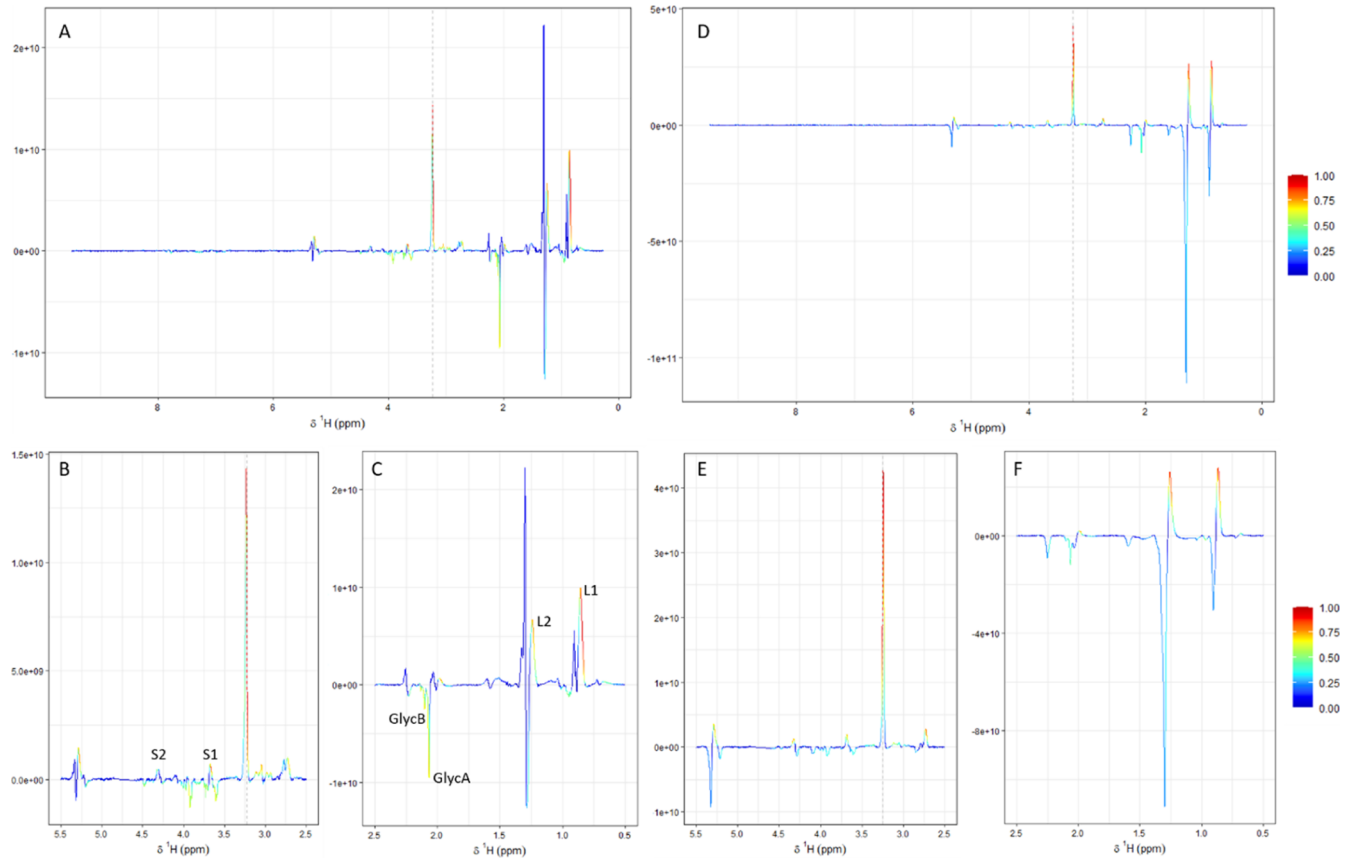

Figure 3. 1D STOCSY of DIRE spectra using SPC-A (δ 3.22) and SPC-B (δ 3.26) as the drivers. (A) 1D STOCSY of the full DIRE spectra using the SPC-A peak as the driver peak to determine the peaks highly correlated (in red). (B) Expanded region δ 2.5−5.5, indicating strong correlation of the driver peak (SPC-A peak) with peaks at δ 3.69 (S1, $\mathrm{NC\mathbf{H}_2CH_2OP-}$) and 4.34 (S2, $\mathrm{NCH_2\mathbf{CH}_2OP-}$). (C) Expanded region δ 0.5−2.5, indicating strong correlation of the driver peak (SPC-A peak) with peaks at δ 0.8 (L1, lysophophatidylcholine CH_3 peak) and δ 1.2 (L2, lysophophatidylcholine CH_2 peak). (D) 1D STOCSY of the full DIRE spectra using the SPC-B peak as the driver peak to determine the peaks highly correlated (in red). (E) Expanded region δ 2.5−5.5, indicating strong correlation of the driver peak with peaks at δ 3.69 and 4.34. (F) Expanded region δ 0.5−2.5, indicating strong correlation of the driver peak, SPC-B, with peaks at δ 0.8 and δ 1.2.

individuals presenting with respiratory symptoms but PCR negative (gray) mapping closer to controls (Figure 2A). Individuals that had tested seropositive but had not been tested for COVID-19 disease (green) were mapped within the space occupied by the control group, with the exception of one individual who mapped with the SARS-CoV-2 positive cluster. This individual had suffered a bout of extreme fatigue after an international trip 4 months earlier and was *post hoc* diagnosed as having COVID-19 with metabolic abnormalities at the time of testing. Whereas the sample distribution in the first principal component (PC) was attributable to variation in triglycerides (Figure 2B), the inherent differences in the molecular composition of plasma from SARS-CoV-2 PCR-positive patients and controls were defined in the second PC, and the vector relating to SARS-CoV-2 infection was driven by the increased intensity of the *N*-acetylglycoprotein signals GlycA and GlycB and the decreased intensity of a signal representing a phospholipid composite $^{+}N-(CH_3)_3$ (Figure 2C). In order to clarify further the key molecular drivers of the differential SARS-CoV-2 signature, the data were modelled using O-PLS-DA (one predictive + one orthogonal component) using a relatively small subset of the control (n = 7) *versus* SARS-CoV-2 positive (N = 7) spectral data set (Figure 2D).

Strong differentiation between the two groups and the projection of the remaining healthy (n = 21) and SARS-CoV-2-positive (n = 51) samples onto the training set (Figure 2F,G, respectively) effectively achieved perfect classification (AUROC = 1). The projections of the COVID-19 negative and the "recovered" seropositive individuals are shown in Figure 2H,I and do not classify well with either healthy or SARS-Cov-2 positive training set clusters as would be expected, indicating that they were biochemically distinct from both the healthy controls and SARS-CoV-2 positive infected groups. The O-PLS-DA model confirmed the observation from the PCA model that the main signature for SARS-CoV-2 positivity was dominated by signals relating to three main entities GlycA, GlycB (both higher in SARS-CoV-2 positive individuals), and the composite phospholipid signal, SPC (higher in healthy controls). We employed NMR and statistical correlation tools to further elucidate the molecular components of the SPC peaks and establish the statistical relationships between the candidate biomarker peaks.

Differential Diagnostic Information in DIRE NMR Spectra. DIRE spectra of blood plasma give a clear and unequivocal modelling diagnostic for SARS-CoV-2 infection. Thus, the key molecular contributors to the SARS-CoV-2 diagnostic in the DIRE spectra were the *N*-acetylglycoprotein peaks GlycA and GlycB and one of the major components of the composite DIRE signals at δ 3.20−3.30. This signal comes partly from a molecule with the same molecular diffusion constant as

https://dx.doi.org/10.1021/acs.analchem.0c04952
Anal. Chem. 2021, 93, 3976−3986

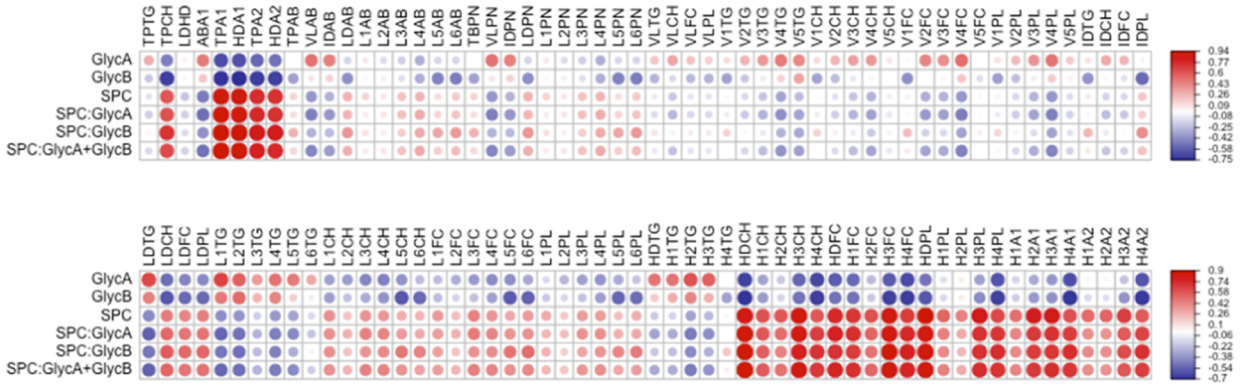

Figure 4. Spearman's ranked correlation plots of the IVDr-derived lipoprotein data with the GlycA, GlycB, and SPC_{total} integrals (obtained from the DIRE spectra), color, and size scaled to magnitude of correlations. Red indicates positive and blue indicates negative correlations. Only significant correlations with a p-value <0.05 are shown, with blank squares indicating no significant difference after correcting for multiple testing. Lipoprotein nomenclature can be found in Table S6.

Table 1. Relative Intensity Group Medians for GlycA, GlycB, SPC Signal Variables, and Their Ratios and Kruskal–Wallis Rank Sum Test p Values for Differences in Healthy Controls and SARS-CoV-2 Negative Patients, SARS-CoV-2 Negative Patients *versus* SARS-CoV-2 Positive Patients, and Healthy Controls and SARS-CoV-2 Positive Patients[a]

spectral variable	healthy controls (n = 26)	SARS-CoV-2 negative patients (n = 34)	SARS-CoV-2 positive patients (n = 17, 58 samples)	P value controls *vs* SARS-CoV-2 negative	P value SARs-CoV-2 negative *vs* SARS-CoV-2 positive	P value Controls *vs* SARS-CoV-2 positive
GlycA (intensity)	1.67×10^7 [1.35×10^7–2.20×10^7]	1.78×10^7 [1.31×10^7–2.68×10^7]	2.18×10^7 [1.70×10^7–2.70×10^7]	0.11 (NS)	4.94×10^{-6}	2.52×10^{-10}
GlycB (intensity)	3.28×10^6 [2.40×10^6–4.39×10^6]	3.66×10^7 [3.01×10^6–5.68×10^6]	5.15×10^6 [3.35×10^6–7.66×10^6]	0.14 (NS)	9.24×10^{-9}	1.25×10^{-9}
GlycA plus GlycB (intensity)	2.00×10^7 [1.64×10^7–3.44×10^7]	2.18×10^7 [1.62×10^7–3.02×10^7]	2.63×10^7 [2.13×10^7–3.44×10^7]	0.09 (NS)	4.86×10^{-7}	1.64×10^{-10}
SPC_{total} (intensity)	3.72×10^7 [2.52×10^7–4.61×10^7]	3.53×10^7 [2.38×10^7–5.12×10^7]	2.62×10^7 [1.54×10^7–4.15×10^7]	0.60 (NS)	4.52×10^{-8}	1.40×10^{-7}
SPC_{total}/GlycA	2.05 [1.61–3.03]	1.98 [1.06–3.30]	1.19 [0.67–1.91]	0.21 (NS)	1.60×10^{-9}	1.23×10^{-10}

[a]All p values were determined using the Kruskal–Wallis rank sum test. Key: GlycA/B: *N*-acetyl glycoprotein fragment A/B; SPC_{total}: supramolecular phospholipid complex total signal; NS = not significant.

GlycA and GlycB, the most likely candidate being linoleoyl-phosphatidylcholine based on its chemical shifts and known abundance (Figures S8, S9, and S10). Moreover it is established that lysophosphatidylcholines in serum and plasma are known to bind and be carried by α-1-acid glycoprotein,[41] which is the main contributor to the GlycA signal[21] and, therefore, expected to have the same molecular diffusion properties. A second component of the SPC signal is likely to be the phospholipid present in high-density lipoprotein (HDL) domains based on the statistical correlations with the IVDr-derived lipoprotein data from the same samples (Figure 4). The DIRE spectra show strong signals from these phosphatidylcholine species including the $N^+–(CH_3)_3$ head groups of compartmentalized phospholipids and signals from partially unsaturated fatty acid side chains. The triglyceride signals observed in DIRE spectra carried little direct diagnostic information, being more closely reflective of body mass index than infection status.[3,42] On closer inspection of the NMR data, SPC was seen to be composed of two major signals with separate average chemical shifts and linewidths (Figure 1). We designated these peaks as SPC-A and SPC-B in an analogous fashion to the composite peak designation of GlycA and GlycB, and we deduced that these originated from the different contributions from the low-density lipoprotein (LDL), HDL/glycoprotein bound phospholipids in each signal, see Supporting Information. The summed total of the SPC-A and SPC-B signals, designated SPCtotal were used in the statistical analysis (Table 1). While the glycoprotein components show a strong positive association with SARS-CoV-2 infection, the total terminal head group phosphatidylcholine signals SPC_{total} at δ 3.20–3.30 are significantly reduced in SARS-CoV-2 positive patients in comparison with controls (Figure 1). α-1-acid glycoprotein and the related acute phase reactive protein are elevated in a variety of inflammatory conditions,[21,43,44] and we have reported significant elevations in SARS-CoV-2 positive patients.[3,42]

The GlycA signal contains contributions from α-1-acid glycoprotein, accounting for most of the intensity, with lesser contributions from a composite of signals from α-1-antichymotrypsin, α-1-antitrypsin, haptoglobin, and transferrin.[21] The role of α-1-acid glycoprotein in binding a range of lysophosphatidylcholines in a 1:1 molar ratio as well as small lipophilic molecules has previously been established[41] and partially explains the observation that the signals from GlycA and the composite SPC signal have the same molecular diffusion constant. However, in contrast to GlycA and GlycB, which increase as a response to SARS-CoV-2 infection, several lysophosphatidylcholine species decrease as reported previously.[3,42,45] This contrasting behavior is captured in the O-PLS-DA coefficient plot (Figure 2).

STOCSY Analysis of DIRE Spectra. STOCSY allows structural connectivity to be established based on the covariance of proton signals from the same molecules across a series of

https://dx.doi.org/10.1021/acs.analchem.0c04952
Anal. Chem. 2021, 93, 3976–3986

spectra collected in parallel.[11] STOCSY analysis of the DIRE spectra using the GlycA signal (δ 2.03) as the statistical driver peak statistically illuminated various structurally correlated signals from other glycan protons from GlycA in the region from δ 3.5 to 4.3 with the highest correlations (>0.9) at δ 3.7 and δ 3.9 (Figures S5 and S8) from the sugar ring protons. Second, GlycB can be observed highly correlated at δ 2.07, which is expected as GlycB presents different acetyl residues (here: *N*-acetylneuraminidino groups) located on the same proteins.

STOCSY analysis driven from the SPC-A signal at δ 3.22 shows a more extensive correlation landscape (Figure 3A) including a highly correlated group of signals at δ 0.80, 1.25, 1.90, 2.7, 3.71, 4.0, and 5.4. Broad resonances around δ 3.2 in 1D plasma proton NMR spectra present trimethylammonium headgroups of choline moieties from phospholipids, for example, phosphatidylcholines or sphingomyelins.[8] The observed STOCSY signal pattern is in good agreement with the expected chemical shifts for phosphatidylcholines as the signals at δ 3.69 and δ 4.34 correspond to the methylene groups in the choline moiety and the remaining signals belong to the attached alkyl chain. Notably, the shift for the signals at δ 0.8 and δ 1.3 matches the literature shifts[7] for HDL particles, indicating that the STOCSY-highlighted phosphatidylcholine might be incorporated in HDL. Special attention is given to the complex multiplet signal at *ca.* δ 2.7 (Figure 3) as it is characteristic for a methylene (sp^3 carbon) group in between the two sp^2 methine carbons, indicating that at least one linoleyl lysophosphatidylcholine species is observed in these STOCSY data. This is consistent with known binding propensities of α_1-acid-glycoprotein and the observation of such bound species.[41]

To corroborate the results from the STOCSY analysis, titrations of potential candidate molecules matching the observed signals were carried out. Figure S7 shows the addition of α_1-acid glycoprotein into human plasma resulting in a signal increase at δ 2.03 and δ 2.07 corresponding to the composite signals of GlycA and GlycB as the α_1-acid glycoprotein presents its main composite, as described previously. Additionally, a set of signals between δ 3.5 and 4.1 can be observed, corresponding to various sugar ring moieties of the oligosaccharides from the glycoprotein. Comparison of STOCSY and the DIRE-difference spectrum with α1-acid glycoprotein as the standard (Figure S10) shows a good overlap of both spectra, confirming that some signals in a DIRE spectrum come from the various glycoproteins that comprise GlycA and GlycB. Furthermore, the DIRE difference spectrum shows a small but distinct resonance at δ 3.22 corresponding to SPC-A and two broad resonances at δ 0.9 and δ 1.3, further suggesting a possible binding interaction of the α-1-acid glycoprotein with phosphatidylcholines and HDL particles.

In order to confirm the identity of the choline moiety unambiguously, a set of hetero- and homonuclear NMR experiments were performed. First, the superimposition of edited $^1H^{13}C$-heteronuclear single quantum coherence (HSQC) and an $^1H^{13}C$-heteronuclear multiple bond correlation (HMBC) shows a clear HMBC cross-peak to $\delta^{13}C$ 68.6 between the choline headgroup $-N^+-(CH_3)_3$ signal belonging to SPC at $\delta^{13}C$ 56.6 and the closest methylene group in the choline moiety (Figure S6). Second, a DE-TOCSY NMR spectrum was acquired (Figure S7) that shows a correlation between the two choline methylene groups at δ 3.69 and δ 4.34. With this information, the second methylene group can be assigned to the CH_2 at δ 62.1 (δ ^{13}C) in the HSQC spectrum of blood plasma (Figure S6).

To get further insight into the nature of the phosphatidylcholine signals highlighted by STOCSY, titrations of various phosphatidylcholine standards into plasma were performed (Figure S8A–D). All tested standards give rise to a similar signal pattern with an observable increase of SPC (SPC-A: δ 3.22 SPC-B: δ 3.26) as well as two signals at δ 3.69 and δ 4.34 corresponding to the methylene groups in the choline moiety. Additionally, signals at δ 0.8, 1.3, 2.0, and 5.3 increased, matching the respective alkyl chain of the investigated standard.

The l-α-lysophosphatidylcholine shows a significant high-frequency shift of 16 Hz for the methylene group flanking the phospho-ester compared to STOCSY, suggesting that the STOCSY signal pattern indicates a saturated phosphatidylcholine form with two aliphatic chains such as dipalmitoyl-phosphatidylcholine, and it is likely that there are several saturated and unsaturated species present. The difference spectrum obtained by subtraction of the standard 1D NMR experiment before and after standard titration provides a clear spectrum of the standard with stoichiometric ratios for each signal. This suggests that all added standards are bound and incorporated into various lipoprotein particles restricting the molecular motions of the different phosphatidylcholine moieties. As the chemical shifts of the signals at δ 0.8 and δ 1.3 closely match the shifts observed in isolated LDL particles,[12] it can be assumed that the detectable signals from the standards arise after incorporation into HDL particles. As all standards yield a similar spectral pattern which matches the STOCSY analysis, it can be assumed that SPC_{total} presents a combination of multiple phosphatidylcholine species including saturated, unsaturated phosphocholine, as well as their lyso-forms mainly located in HDL particles. Comparison of STOCSY and the DIRE-difference spectrum with 1,2-dilinoleoyl-sn-glycero-3-phosphocholine as the standard (Figure S11) shows a near perfect overlap of both spectra confirming that a significant portion of signals in the DIRE spectrum come from phosphatidylcholines with a high proportion of unsaturated species.

Both the relative intensities of GlycA and GlycB and their sums give extremely good discrimination between healthy and SARS-CoV-2 positive individuals with Kruskal–Wallis *p*-values in the 10^{-9} to 10^{-10} range (Table 1). The differences for healthy *versus* SARS-CoV-2 negative and controls were significant but much weaker, as were the differences between SARS-CoV-2 negatives and positives. None of these parameters were significantly different between healthy and SARS-CoV-2 negative patients (Table 1). The SPC composite peak also strongly distinguished controls from SARS-CoV-2 positives ($p = 1.40 \times 10^{-7}$ and more importantly, between SARS-CoV-2 negative respiratory patients *vs* SARS-CoV-2 positives ($p = 4.52 \times 10^{-8}$), indicating that this novel peak has a differential diagnostic value. The SPC and GlycA have opposite signs, and so the SPC: GlycA ratio was also highly significant for SARS-CoV-2 positives *versus* healthy or SARS-CoV-2 negatives, which makes this ratio a highly specific and sensitive diagnostic for SARS-CoV-2 induced metabolic phenoconversion.

We investigated the statistical relationships between the measured GlycA, GlycB, and SPC_{total} signals and the IVDr lipoprotein parameters derived from the same samples by the standard B.I.LISA method.[37] We have previously shown the complex relationships between the lipoprotein patterns and other metabolic and cytokine data from COVID-19 patients, noting the inflammatory driven connections to COVID-19 dyslipidemia (elevated VLDL and LDL and elevated apolipo-

https://dx.doi.org/10.1021/acs.analchem.0c04952
Anal. Chem. 2021, 93, 3976–3986

protein B100/A1 and their possible implications in new onset diabetes and cardiovascular/atherosclerotic risk).[39] Here, we are using the lipoprotein data to establish a structural and compartmental connectivity to the novel SPC_{total} data and the SPC_{total}/glycoprotein ratios. A strong pattern of correlation emerges between the SPC_{total} and total plasma and the total HDL apolipoprotein A1 and A2 levels. This is because a significant proportion of the plasma apolipoproteins are carried on HDL, which is significantly reduced in COVID-19. Similarly, there is a strong correlation between the SPC_{total} signal and multiple HDL fraction concentrations because the HDL phospholipids are in the same structural compartment, as for instance, the free cholesterol and total cholesterol. The exception is the weaker correlations with HDL-1 and HDL-2 fractions (phospholipids and cholesterol) because these are much less reduced in the disease. Thus, we infer that a significant proportion of the SPC_{total} component is present in the HDL subfraction 3 and HDL subfraction 4. There is also a correlation between the SPC_{total} peak and the LDL-3, LDL-4, LDL-5, and LDL-6 peaks, but these are much weaker than the HDL correlations. So, on the basis of the DE-STOCSY experiment and the statistical IVDr correlations, we can conclude that the main composite SPC_{total} diagnostic markers are from phospholipids in HDL-3 and HDL-4 with a contribution from the lysophoshatidylcholine (including a linoleolyl, 18:2 species) bound to α_1-1-acid glycoprotein, both of which are significantly lowered in COVID-19 disease. The fact that the α_1-1-acid glycoprotein is significantly elevated in COVID-19 as part of the inflammatory response makes the various ratios of GlycA/GlycB and SPC components particularly sensitive to the presence of the disease (Table 1). These data also well illustrate how untargeted NMR spectroscopic exploration can be readily translated into targeted measurements that can be performed on the same sample within the same experiment.

The fundamental molecular basis of these NMR-detected COVID-19 responses is as yet unknown, but the driving force of the pathology and individual severity and persistence is the integrated immune response.[46] It will be important to determine the relative contribution of both cellular and humoral responses of the disease to the observed metabolic changes observed here and from other methods[3,39,42] in order to fully understand the complex immunometabolic landscape and dynamics of SARS-CoV-2 infections.

CONCLUSIONS

We have shown that a combination of diffusion and relaxation NMR spectroscopy of blood plasma provides excellent discrimination of SARS-CoV-2 positivity from controls or SARS-CoV-2 negative respiratory patients based on the enhanced detection of NMR signals from occult diagnostic compartments. The key diagnostic species are from the total composite NMR signals (SPC) from terminal head groups in phospholipids from HDL, especially subfractions HDL-3 and HDL-4, together with lysophosphatidylcholine bound to α-1-acid glycoprotein and the glycoprotein *N*-acetyl composite signals GlycA and GlycB. SPC has two distinguishable components (SPC-A and SPC-B) based on chemical shifts and linewidths; these carry different, but related, diagnostic information, and further experiments are required to investigate if these separate signals have any deeper differential diagnostic value. The SPC/Glyc ratios appear to offer excellent diagnostic discrimination, and the high speed (4.5 min) of the DIRE experiment could be exploited to provide a direct phenoconversion test to help augment conventional PCR tests and hence would be of potential value in biosecurity applications, but this requires further validation. Although our data indicate that mild non-COVID-19 respiratory disease is well discriminated by the DIRE method, differentiation from influenza and related diseases has yet to be tested. For many COVID-19 patients, recovery is slow or incomplete and DIRE spectra or SPC/Glyc ratios could also be employed as measures of functional systemic recovery. The DIRE diagnostic is unusual in that it utilizes the dynamic motional properties of the biomarker molecules as well as concentration variations to enhance classification of the disease over methods employing simple concentration metrics and thus represents a new class of molecular dynamic diagnostic.

ASSOCIATED CONTENT

Supporting Information

The Supporting Information is available free of charge at https://pubs.acs.org/doi/10.1021/acs.analchem.0c04952.

Cohort demographic data and pathological associations of GlycA and GlycB; quantification of lipoproteins; diffusion and relaxation editing; GlycA, GlycB, SPC integrals, and STOCSY analysis; 2D NMR experiments; and titration of phospholipid standards and α-1-acid glycoprotein (PDF)

AUTHOR INFORMATION

Corresponding Authors

Elaine Holmes − *Australian National Phenome Center, and Center for Computational and Systems Medicine, Health Futures Institute, Murdoch University, Perth WA6150, Australia; Department of Metabolism, Digestion and Reproduction, Faculty of Medicine, Imperial College London, London SW7 2AZ, U.K.;* orcid.org/0000-0002-0556-8389; Email: Elaine.Holmes@murdoch.edu.au

Jeremy K. Nicholson − *Australian National Phenome Center, and Center for Computational and Systems Medicine, Health Futures Institute, Murdoch University, Perth WA6150, Australia; Division of Surgery, Medical School, Faculty of Health and Medical Sciences, University of Western Australia, Perth WA6150, Australia; Institute of Global Health Innovation, Faculty of Medicine, Imperial College London, London SW7 2NA, U.K.*; Email: Jeremy.Nicholson@murdoch.edu.au

Authors

Samantha Lodge − *Australian National Phenome Center, and Center for Computational and Systems Medicine, Health Futures Institute, Murdoch University, Perth WA6150, Australia;* orcid.org/0000-0001-9193-0462

Philipp Nitschke − *Australian National Phenome Center, and Center for Computational and Systems Medicine, Health Futures Institute, Murdoch University, Perth WA6150, Australia*

Torben Kimhofer − *Australian National Phenome Center, and Center for Computational and Systems Medicine, Health Futures Institute, Murdoch University, Perth WA6150, Australia;* orcid.org/0000-0001-7158-9930

Julien Wist − *Australian National Phenome Center, and Center for Computational and Systems Medicine, Health Futures Institute, Murdoch University, Perth WA6150, Australia; Chemistry Department, Universidad del Valle, Cali 76001, Colombia;* orcid.org/0000-0002-3416-2572

https://dx.doi.org/10.1021/acs.analchem.0c04952
Anal. Chem. 2021, 93, 3976−3986

Sze-How Bong − *Australian National Phenome Center, and Center for Computational and Systems Medicine, Health Futures Institute, Murdoch University, Perth WA6150, Australia;* orcid.org/0000-0002-3313-5097
Ruey Leng Loo − *Australian National Phenome Center, and Center for Computational and Systems Medicine, Health Futures Institute, Murdoch University, Perth WA6150, Australia;* orcid.org/0000-0001-5307-5709
Reika Masuda − *Australian National Phenome Center, and Center for Computational and Systems Medicine, Health Futures Institute, Murdoch University, Perth WA6150, Australia*
Sofina Begum − *Australian National Phenome Center, and Center for Computational and Systems Medicine, Health Futures Institute, Murdoch University, Perth WA6150, Australia; Department of Metabolism, Digestion and Reproduction, Faculty of Medicine, Imperial College London, London SW7 2AZ, U.K.*
Toby Richards − *Division of Surgery, Medical School, Faculty of Health and Medical Sciences, University of Western Australia, Perth WA6150, Australia*
John C. Lindon − *Department of Metabolism, Digestion and Reproduction, Faculty of Medicine, Imperial College London, London SW7 2AZ, U.K.;* orcid.org/0000-0002-0916-6360
Wolfgang Bermel − *Bruker Biospin GmbH, Ettlingen 76275, Germany*
Tony Reinsperger − *Bruker Biospin GmbH, Ettlingen 76275, Germany*
Hartmut Schaefer − *Bruker Biospin GmbH, Ettlingen 76275, Germany*
Manfred Spraul − *Bruker Biospin GmbH, Ettlingen 76275, Germany*

Complete contact information is available at: https://pubs.acs.org/10.1021/acs.analchem.0c04952

Notes

The authors declare no competing financial interest.

■ ACKNOWLEDGMENTS

We thank The Spinnaker Health Research Foundation, WA, The McCusker Foundation, WA, The Western Australian State Government, and the MRFF for funding the Australian National Phenome Centre for this and related work. We thank the UK MRC for funding (SB), the Department of Jobs, Tourism, Science and Innovation, Government of Western Australian Premier's Fellowship for funding R.L.L. and E.H., and the ARC Laureate Fellowship funding for E.H. We also would like to acknowledge the Western Australian Covid Research Response team (https://research-au.net/covid-research-response/), Dale Edgar, Giuliana D'Aulerio, Kelly Beer, Rolee Kumar, Doug Robb, Joseph Miocevich, Dominic Mallonic, Michael Epis, Merrilee Needham, Daniel Fatovich, Aron Chakera, Thomas Gilbert, Nathanael Foo, @STRIVE WA, Candice Peel, Sheeraz Mohd, and Ali Alishum for the coordination, sampling, and biobanking of patient samples and clinical metadata.

■ REFERENCES

(1) Holmes, E.; Wilson, I. D.; Nicholson, J. K. *Cell* **2002**, *134*, 714−717.
(2) Nicholson, J. K.; Connelly, J.; Lindon, J. C.; Holmes, E. *Nat. Rev. Drug Discov.* **2002**, *1*, 153−161.
(3) Kimhofer, T.; Lodge, S.; Whiley, L.; Gray, N.; Loo, R. L.; Lawler, N. G.; Nitschke, P.; Bong, S.-H.; Morrison, D. L.; Begum, S.; Richards, T.; Yeap, B. B.; Smith, C.; Smith, K. G. C.; Holmes, E.; Nicholson, J. K. *J. Proteome Res.* **2020**, *19*, 4442−4454.
(4) Nicholson, J. K.; O'Flynn, M. P.; Sadler, P. J.; Macleod, A. F.; Juul, S. M.; Sönksen, P. H. *Biochem. J.* **1984**, *217*, 365−375.
(5) Nicholson, J. K.; Wilson, I. D. *Prog. Nucl. Magn. Reson. Spectrosc.* **1989**, *21*, 449−501.
(6) Nicholson, J. K.; Holmes, E.; Kinross, J. M.; Darzi, A. W.; Takats, Z.; Lindon, J. C. *Nature* **2012**, *491*, 384−392.
(7) Bell, J. D.; Sadler, P. J.; Macleod, A. F.; Turner, P. R.; La Ville, A. *FEBS Lett.* **1987**, *219*, 239−243.
(8) Nicholson, J. K.; Foxall, P. J. D.; Spraul, M.; Farrant, R. D.; Lindon, J. C. *Anal. Chem.* **1995**, *67*, 793−811.
(9) Posma, J. M.; Garcia-Perez, I.; De Iorio, M.; Lindon, J. C.; Elliott, P.; Holmes, E.; Ebbels, T. M. D.; Nicholson, J. K. *Anal. Chem.* **2012**, *84*, 10694−10701.
(10) Robinette, S. L.; Lindon, J. C.; Nicholson, J. K. *Anal. Chem.* **2013**, *85*, 5297−5303.
(11) Cloarec, O.; Dumas, M.-E.; Craig, A.; Barton, R. H.; Trygg, J.; Hudson, J.; Blancher, C.; Gauguier, D.; Lindon, J. C.; Holmes, E.; Nicholson, J. *Anal. Chem.* **2005**, *77*, 1282−1289.
(12) Daykin, C. A.; Foxall, P. J. D.; Connor, S. C.; Lindon, J. C.; Nicholson, J. K. *Anal. Biochem.* **2002**, *304*, 220−230.
(13) Daykin, C. A.; Corcoran, O.; Hansen, S. H.; Bjørnsdottir, I.; Cornett, C.; Connor, S. C.; Lindon, J. C.; Nicholson, J. K. *Anal. Chem.* **2001**, *73*, 1084−1090.
(14) Clerc, F.; Reiding, K. R.; Jansen, B. C.; Kammeijer, G. S. M.; Bondt, A.; Wuhrer, M. *Glycoconj. J.* **2016**, *33*, 309−343.
(15) Levine, J. A.; Han, J. M.; Wolska, A.; Wilson, S. R.; Patel, T. P.; Remaley, A. T.; Periwal, V.; Yanovski, J. A.; Demidowich, A. P. *J. Clin. Lipidol.* **2020**, *14*, 667−674.
(16) Akinkuolie, A. O.; Pradhan, A. D.; Buring, J. E.; Ridker, P. M.; Mora, S. *Arterioscler. Thromb. Vasc. Biol.* **2015**, *35*, 1544−1550.
(17) Gruppen, E. G.; Riphagen, I. J.; Connelly, M. A.; Otvos, J. D.; Bakker, S. J. L.; Dullaart, R. P. F. *PLoS One* **2015**, *10*, No. e0139057.
(18) Rodriguez-Carrio, J.; Alperi-Lopez, M.; Lopez, P.; Perez-Alvarez, A. I.; Gil-Serret, M.; Amigo, N.; Ulloa, C.; Benavente, L.; Ballina-Garcia, F. J.; Suarez, A. *J. Clin. Med.* **2020**, *9*, 2472.
(19) Malo, A.-I.; Rull, A.; Girona, J.; Domingo, P.; Fuertes-Martin, R.; Amigo, N.; Rodriguez-Borjabad, C.; Martinez-Micaelo, N.; Leal, M.; Peraire, J.; Correig, X.; Vidal, F.; Masana, L. *J. Clin. Med.* **2020**, *9*, 1344.
(20) Chung, C. P.; Ormseth, M. J.; Connelly, M. A.; Oeser, A.; Solus, J. F.; Otvos, J. D.; Raggi, P.; Stein, C. M. *Lupus* **2016**, *25*, 296−300.
(21) Otvos, J. D.; Shalaurova, I.; Wolak-Dinsmore, J.; Connelly, M. A.; Mackey, R. H.; Stein, J. H.; Tracy, R. P. *Clin. Chem.* **2015**, *61*, 714−723.
(22) Taguchi, K. N. K.; Chuang, V. T. M.; Maruyama, T.; Otagiri, M. *Molecular Aspects of Human Alpha-1 Acid Glycoprotein-Structure and Function*, 2013.
(23) Bories, P. N.; Kodari, E.; Feger, J.; Rouzeau, J. D.; Agneray, J.; Durand, G. *Immunol. Lett.* **1990**, *26*, 105−110.
(24) Elg, S. A.; Mayer, A. R.; Carson, L. F.; Twiggs, L. B.; Hill, R. B.; Ramakrishnan, S. *Cancer* **1997**, *80*, 1448−1456.
(25) Hochepied, T.; Berger, F. G.; Baumann, H.; Libert, C. *Cytokine Growth Factor Rev.* **2003**, *14*, 25−34.
(26) Williams, J. P.; Weiser, M. R.; Pechet, T. T. V.; Kobzik, L.; Moore, F. D., Jr.; Hechtman, H. B. *Am. J. Physiol.* **1997**, *273*, G1031−G1035.
(27) Gambacorti-Passerini, C.; Zucchetti, M.; Russo, D.; Frapolli, R.; Verga, M.; Bungaro, S.; Tornaghi, L.; Rossi, F.; Pioltelli, P.; Pogliani, E.; Alberti, D.; Corneo, G.; D'Incalci, M. *Clin. Cancer Res.* **2003**, *9*, 625−632.
(28) Ritchie, S. C.; Würtz, P.; Nath, A. P.; Abraham, G.; Havulinna, A. S.; Fearnley, L. G.; Sarin, A.-P.; Kangas, A. J.; Soininen, P.; Aalto, K.; Seppälä, I.; Raitoharju, E.; Salmi, M.; Maksimow, M.; Männistö, S.; Kähönen, M.; Juonala, M.; Ripatti, S.; Lehtimäki, T.; Jalkanen, S.; Perola, M.; Raitakari, O.; Salomaa, V.; Ala-Korpela, M.; Kettunen, J.; Inouye, M. *Cell Syst.* **2015**, *1*, 293−301.

(29) Lorenzo, C.; Festa, A.; Hanley, A. J.; Rewers, M. J.; Escalante, A.; Haffner, S. M. *Diabetes Care* **2017**, *40*, 375−382.
(30) Nicholson, J. K.; Buckingham, M. J.; Sadler, P. J. *Biochem. J.* **1983**, *211*, 605−615.
(31) Morris, K. F.; Johnson, C. S. *J. Am. Chem. Soc.* **1992**, *114*, 3139−3141.
(32) Nilsson, M.; Duarte, I. F.; Almeida, C.; Delgadillo, I.; Goodfellow, B. J.; Gil, A. M.; Morris, G. A. *J. Agric. Food Chem.* **2004**, *52*, 3736−3743.
(33) Griffin, J. *Curr. Opin. Chem. Biol.* **2003**, *7*, 648−654.
(34) Liu, M.; Nicholson, J. K.; Lindon, J. C. *Anal. Chem.* **1996**, *68*, 3370−3376.
(35) Liu, M.; Nicholson, J. K.; Parkinson, J. A.; Lindon, J. C. *Anal. Chem.* **1997**, *69*, 1504−1509.
(36) Dona, A. C.; Jiménez, B.; Schäfer, H.; Humpfer, E.; Spraul, M.; Lewis, M. R.; Pearce, J. T. M.; Holmes, E.; Lindon, J. C.; Nicholson, J. K. *Anal. Chem.* **2014**, *86*, 9887−9894.
(37) Jiménez, B.; Holmes, E.; Heude, C.; Tolson, R. F.; Harvey, N.; Lodge, S. L.; Chetwynd, A. J.; Cannet, C.; Fang, F.; Pearce, J. T. M.; Lewis, M. R.; Viant, M. R.; Lindon, J. C.; Spraul, M.; Schäfer, H.; Nicholson, J. K. *Anal. Chem.* **2018**, *90*, 11962−11971.
(38) Wei, T. S. V. *R Package "corrplot": Visualization of a Correlation Matrix*, version 0.84, https://github.com/taiyun/corrplot, 2017.
(39) Lodge, S.; Nitschke, P.; Kimhofer, T.; Coudert, J. D.; Begum, S.; Bong, S. H.; Richards, T.; Edgar, D.; Raby, E.; Spraul, M.; Schaefer, H.; Lindon, J. C.; Loo, R. L.; Holmes, E.; Nicholson, J. K. *J. Proteome Res.* **2021**, *20*, 1382−1396.
(40) Wang, Y.; Cloarec, O.; Tang, H.; Lindon, J. C.; Holmes, E.; Kochhar, S.; Nicholson, J. K. *Anal. Chem.* **2008**, *80*, 1058−1066.
(41) Ojala, P. J.; Hermansson, M.; Tolvanen, M.; Polvinen, K.; Hirvonen, T.; Impola, U.; Jauhiainen, M.; Somerharju, P.; Parkkinen, J. *Biochemistry* **2006**, *45*, 14021−14031.
(42) Loo, R. L.; Lodge, S.; Kimhofer, T.; Bong, S.-H.; Begum, S.; Whiley, L.; Gray, N.; Lindon, J. C.; Nitschke, P.; Lawler, N. G.; Schäfer, H.; Spraul, M.; Richards, T.; Nicholson, J. K.; Holmes, E. *J. Proteome Res.* **2020**, *19*, 4428−4441.
(43) Tibuakuu, M.; Fashanu, O. E.; Zhao, D.; Otvos, J. D.; Brown, T. T.; Haberlen, S. A.; Guallar, E.; Budoff, M. J.; Palella, F. J., Jr.; Martinson, J. J.; Akinkuolie, A. O.; Mora, S.; Post, W. S.; Michos, E. D. *AIDS* **2019**, *33*, 547−557.
(44) Bell, J. D.; Brown, J. C. C.; Nicholson, J. K.; Sadler, P. J. *FEBS Lett.* **1987**, *215*, 311−315.
(45) Cai, Y.; Kim, D. J.; Takahashi, T.; Broadhurst, D. I.; Ma, S.; Rattray, N. J. W.; Casanovas-Massana, A.; Israelow, B.; Klein, J.; Lucas, C.; Mao, T.; Moore, A. J.; Muenker, C. M.; Silva, J.; Wong, P.; Ko, A. J.; Khan, S. A.; Iwasaki, A.; Johnson, C. H. *Kynurenic Acid Underlies Sex-Specific Immune Responses to COVID-19*; medRxiv, 2020.
(46) Bergamaschi, L.M. F.; Turner, L.; Hanson, A.; Kotagiri, P.; Dunmore, B. J.; Ruffieux, H.; De Sa, A.; Huhn, O.; Wills, M. R.; Baker, S.; Doffinger, R.; Dougan, G.; Elmer, A.; Goodfellow, I. G.; Gupta, R. K.; Hosmillo, M.; Hunter, K.; Kingston, N.; Lehner, P. J.; Mathson, N. J.; Nicholson, J. K.; Petrunkina, A. M.; Richardson, S.; Saunders, C.; Thaventhiran, J. E. D.; Toonen, E. J. M.; Weekes, M. P.; Toshner, M.; Hess, C.; Bradley, J. R.; Lyons, P. A.; Smith, K. G. C.; Cambridge Institute of Therapeutic Immunology and Infectious Disease-National Institute of Health Research (CITIID-NIHR) COVID BioResource COllaboration *Early Immune Pathology and Persisitent Dysregulation Characterise Severe COVID-19*; medRxiv, 2021.

https://dx.doi.org/10.1021/acs.analchem.0c04952
Anal. Chem. 2021, 93, 3976−3986